01 Jan 2004

Evaluation of Microstructure and Superplasticity in Friction Stir Processed 5083 Al Alloy

Indrajit Charit

Rajiv S. Mishra
Missouri University of Science and Technology

Evaluation of microstructure and superplasticity in friction stir processed 5083 Al alloy

I. Charit and R.S. Mishra[a)]
Center for Friction Stir Processing and Department of Metallurgical Engineering,
University of Missouri, Rolla, Missouri 65409

Friction stir processing (FSP) has been developed as a potential grain refinement technique. In the current study, a commercial 5083 Al alloy was friction stir processed with three combinations of FSP parameters. Fine-grained microstructures with average grain sizes of 3.5–8.5 μm were obtained. Tensile tests revealed that the maximum ductility of 590% was achieved at a strain rate of 3×10^{-3} s^{-1} and 530 °C in the 6.5-μm grain size FSP material, whereas for the material with 8.5-μm grain size, maximum ductility of 575% was achieved at a strain rate of 3×10^{-4} s^{-1} and 490 °C. The deformation mechanisms for both the materials were grain boundary sliding (m ~0.5). However, the 3.5-μm grain size material showed maximum ductility of 315% at 10^{-2} s^{-1} and 430 °C. The flow mechanism was solute-drag dislocation glide (m ~0.33). This study indicated that establishing a processing window is crucial for obtaining optimized microstructure for optimum superplasticity.

I. INTRODUCTION

A material that can exhibit >200% tensile elongation prior to its failure is termed as superplastic. The commercial application of superplasticity materializes through superplastic forming technologies. The advantages of superplastic forming are several and rewarding, when compared with conventional forming techniques.[1] Al alloys are gaining more usage in transport applications with the growing demand for lighter, more fuel-efficient vehicles. One of the most widely used alloys in the automotive industry is 5083 Al. Thus, there has been much interest in investigating superplastic characteristics in 5083 Al because of its good corrosion resistance, good weldability, lower density, and moderately high strength. For more than a decade now, two broad approaches have been underway to produce better superplastic 5083 Al. First, various processing techniques have been applied on the base composition of 5083 Al. There have been a number of efforts following conventional rolling-based thermomechanical processing techniques (TMP),[2–7] equal channel angular pressing (ECAP),[8–11] and accumulative roll bonding (ARB).[12] The drawbacks encountered in these approaches have been slower forming rates and/or instability of grain structures at likely superplastic temperatures. Second, new alloy design concepts have been employed to modify the composition of the alloy for achieving superplasticity. Various alloying additions like Cu,[13,14] Mn,[15] Mn + Sc,[16] Sc + Sn,[17] Mn + Zr,[16,18] Zr,[19–21] and Sc[16,22] in base-5083 compositions have been reported. There have been significant improvements in ductility in the modified alloys, however, with the likely complexities during their production and deterioration of other useful properties. The use of these modified alloys also limits easy use of the vast knowledge base of 5083 Al. Hence, the current approach was to use a commercial 5083 Al and make the microstructure amenable for enhanced superplasticity using the friction stir processing (FSP) technique.

FSP is based on the same fundamental principles as the friction stir welding (FSW)[23] and is being developed as a viable grain refinement technique for aluminum alloys. A high strength tool, with a larger diameter shoulder and a smaller diameter pin with threads, is used for friction stirring. The pin plunges into the material and the shoulder contacts the material surface. Heat generated from frictional effects and adiabatic heating from severe plastic deformation softens the material, which is moved from the front to the back of the tool during a weld traverse, and subsequently gets consolidated by the forging action of the tool shoulder. The friction stir processed region has fine, equiaxed grains with high grain boundary misorientations.[24–26] These features are essential for achieving enhanced superplasticity. Excellent superplastic

properties have been achieved in FSP 2024 Al,[26] 7075 Al,[27] Al–4Mg–1Zr,[28] and Al–Zn–Mg–Sc[29] alloys. Based on the success of the previous studies, there is a need for exploring the possibility of enhanced superplasticity in a common, widely used non–heat treatable Al alloy, like 5083 Al. Hence, this study was focused on achieving the following objectives: (i) to investigate the effect of FSP parameters on the microstructural evolution in 5083 Al, (ii) to evaluate the room temperature and elevated temperature mechanical characteristics of the FSP alloys and the parent material in a comparative fashion, (iii) to perform cavitation studies on the deformed tensile specimens to understand the failure mechanisms, and (iv) to interpret the current results in the light of existing superplasticity theories.

II. EXPERIMENTAL

5083 Al alloy was received in the form of as-rolled plates of 6.4-mm thickness. The measured and nominal compositions of the as-received alloy are given in Table I. The plates were friction stir processed using a high strength cobalt alloy (MP159) tool. The tool was fitted with a threaded pin (right-handed screw), and the rotation sense was kept counterclockwise. Tool rotation rate of 400 rpm with traverse speeds of 25.4 mm/min (1 inch/min) and 101.6 mm/min (4 inch/min), respectively, were used for the two runs. Another additional FSP run was made with relatively cold processing parameters (tool rotation rate of 200 rpm and traverse speed of 101.6 mm/min, i.e., 4 inch/min). Throughout this paper, a nomenclature to identify the alloys with their parameters is used, that is, 400/1 identifies the FSP alloy processed with a tool rotation rate of 400 rpm and a traverse speed of 25.4 mm/min (1 inch/min), if not stated otherwise. Likewise, 400/4 and 200/4 will be used to identify the other two FSP alloys. Thermal profile during FSP at a location within the processing path was recorded with a K-type thermocouple. The corresponding temperature profiles are shown in Fig. 1. Table II includes the average tool plunge and traverse forces experienced during the three FSP runs.

The microstructure was observed in a Philips EM430T (Mahwah, NJ) transmission electron microscope operated at 300 kV using jet polished (Tenupol-2 jet polisher, Ballerup, Denmark) foils sampled both from the parent and the FSP materials. The reported grain sizes that were measured from several representative transmission electron microscopy (TEM) micrographs are the average

spatial grain sizes (diameters) determined by mean linear intercept technique (i.e., spatial grain size = 1.78 × mean linear intercept). Primary constituent particles were examined in a JEOL T330A (Peabody, MA) scanning electron microscope in backscattered electron (BSE) mode. Electron backscatter diffraction (EBSD) study was conducted on the electropolished sample using a Zeiss DSM 960 scanning electron microscope (Oxford Instruments EBSD software, Thornwood, NY), in the Center for Microanalysis of Materials (CMM) at the University of Illinois, Urbana-Champaign.

Tensile specimens with gauge length of 1.3 mm and 1.0 mm width were electro-discharge machined and polished to give a final thickness of approximately 0.5 mm. Tensile specimens were tested in a custom-built, computer-controlled tensile tester at constant crosshead speeds. Tensile tests were mainly carried out in the initial strain rate ranges of 10^{-3} to 10^{-1} s^{-1}. It took 30–35 min for heating and temperature stabilization before starting the high temperature tensile test.

Cavitation studies were carried out on unetched, polished cross-sections of the FSP 400/1 5083 Al with the standard optical microscopy. Scion image analysis software (Scion Corporation, Frederick, MD) was used for quantification of cavities.

III. RESULTS

A. Metallographic characterization

Figure 2(a) shows an optical macrograph indicating the FSP zone of the 400/1 5083 Al in a transverse cross-section. The parent microstructure is shown in the TEM micrograph of Fig. 2(b). It shows largely elongated microstructure with both recrystallized and unrecrystallized regions. Figure 2(c) details the unrecrystallized region showing bamboo-type grain structures consisting of fine subgrains and cells (0.5–0.8 μm size). On the other hand, the 400/1 alloy has a fine (average grain size of 6.5 μm), equiaxed, recrystallized microstructure as shown in the TEM micrograph of Fig. 2(d). Fine Al_6(Mn,Cr) particles, 100–300 nm in size, were distributed both in the parent and the FSP alloy, however, the latter has more homogeneous distribution of these particles. Bright-field TEM images of the 200/4 and 400/4 FSP alloys are shown in Figs. 3(a) and 3(b), respectively. The colder processed (200/4) alloy has a finer grain size (3.5 μm), whereas the 400/4 material has an average grain size of ~8.5 μm with some discrete regions having approximately 5.5-μm grain size.

TABLE I. Chemical composition of 5083 Al alloy (in wt. pct).

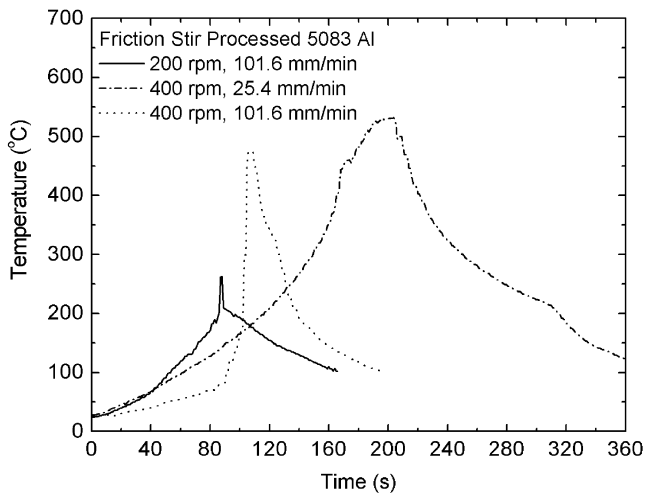| Element	Si	Fe	Cu	Mn	Mg	Zn	Cr	Ti
Measured	0.08	0.13	0.06	0.62	4.10	0.028	0.09	0.019
Nominal	<0.4	<0.4	0.10	0.40–1.0	4.0–4.9	<0.25	0.05–0.25	<0.15

FIG. 1. Temperature profile against time at a point in the tool path during friction stir processing with three different combinations of parameters.

TABLE II. Average plunge and traverse forces measured during friction stir processing of 5083 Al alloys.

Tool rpm/traverse speed	Plunge force (N)	Traverse force (N)
200 rpm, 101.6 mm/min	25,600	4315
400 rpm, 25.4 mm/min	15,340	1295
400 rpm, 101.6 mm/min	23,350	5035

BSE images of both the parent and the FSP (400/1) alloys [Figs. 4(a) and 4(b), respectively] revealed coarse primary intermetallic particles of $Al_6(Mn,Fe)$, Al–Mn–Fe–Si, and Mg_2Si. However, the morphology of these particles was altered by FSP, that is, the size became finer, and the shape more equiaxed.

EBSD examination of both the unprocessed parent region and the FSP 400/1 alloy revealed a large fraction (~85%) of high angle grain boundaries (HAGB), that is, boundary angle >15°, as shown in the histogram of the grain boundary misorientation distribution (GBMD) in Fig. 5. The EBSD data were obtained from the regions of the parent material that statically recrystallized due to thermal cycle to better reflect its microstructural condition just before the start of high temperature tensile straining.

B. Tensile test results

The yield strength, tensile strength and ductility (% elongation to failure) values for the parent material and the FSP materials are listed in Table III. The results reveal a loss in yield strength of the FSP region as compared to that of the parent material. However, the ultimate tensile strength values remain similar. At the same time, the ductility values were at par (for 200/4) or slightly higher (for 400/1 and 400/4) than that of the parent alloy.
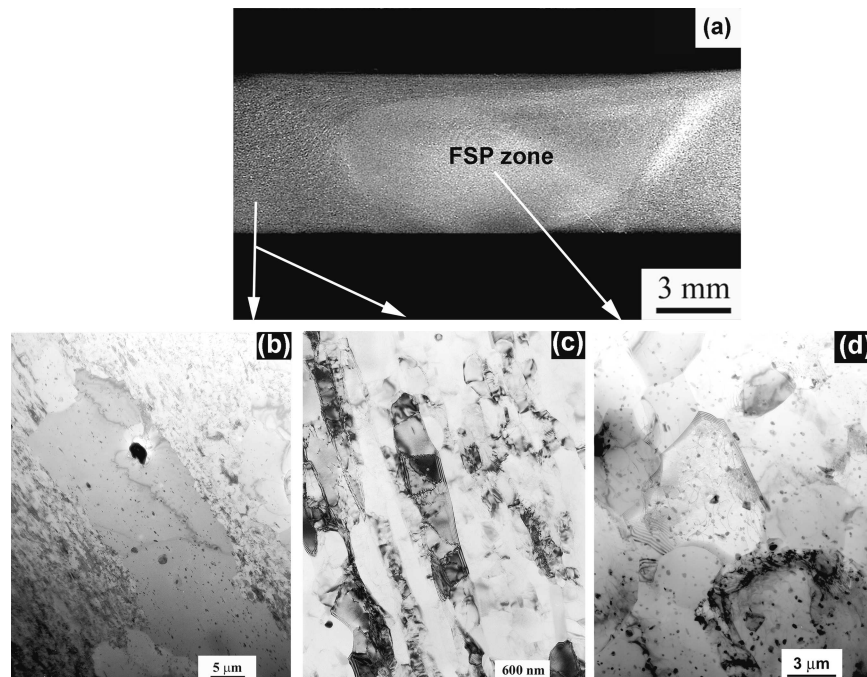

FIG. 2. (a) An optical macrograph showing the transverse cross-sectional view of the FSP 5083 Al (400/1) alloy. (b) A bright-field TEM image of the parent 5083 Al, showing both recrystallized and unrecrystallized regions. (c) An enlarged view of the unrecrystallized region consisting of subgrains. (d) A bright-field TEM micrograph showing grain morphology and particles in an FSP 5083 Al alloy.
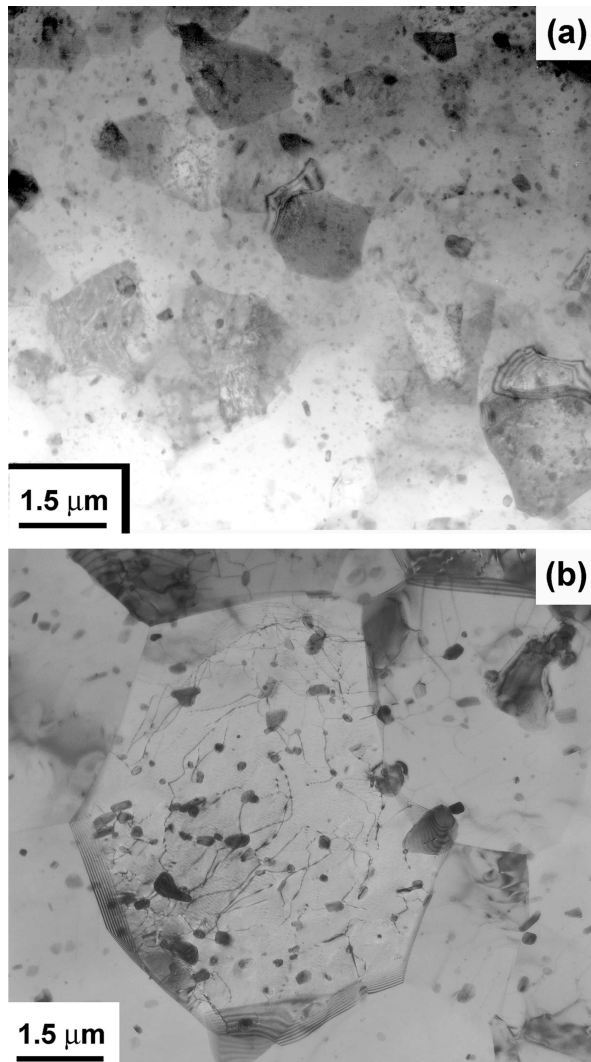
FIG. 3. (a) and (b) TEM images of the FSP 5083 Al alloys processed at a traverse speed of 101.6 mm/min (4 inch/min) and at a tool rotational speed of 200 and 400 rpm, respectively.

FIG. 4. The distribution of constituent particles, Al_6(Mn,Fe) in 5083 Al alloy (a) before FSP and (b) after FSP (400 rpm, 25.4 mm/min, i.e., 400/1).

Figure 6 shows the stress-strain behavior of the parent and the 400/1 FSP materials at 530 °C for two strain rates. With increasing strain rate, the flow hardening regime shortened. However, the flow stresses were consistently lower for the FSP material than those of the parent material. Stress-strain curves of similar nature were also obtained for two other FSP alloys.

Figure 7 shows the variation of ductility with temperature for all the alloys at a strain rate of 10^{-2} s^{-1}. This strain rate was chosen for comparison of the data because this is the widely accepted lower limit of high strain rate superplasticity (HSRS). At this strain rate, the FSP 400/1 material showed the best ductility of 446% at a temperature of 530 °C, whereas that for the FSP 400/4 material was approximately 400% at 490 °C. The highest ductility of 315% was achieved in the 200/4 FSP alloy at a far lower temperature of 430 °C. For comparison, the parent
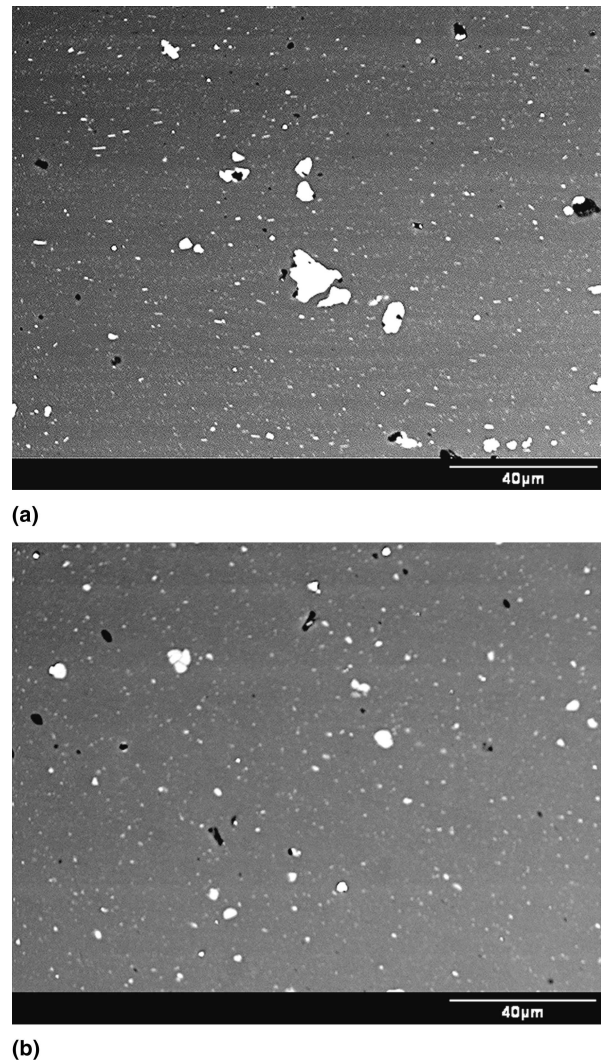
material exhibited maximum elongation of 240% at this strain rate and 530 °C. The variation of flow stress (at a true plastic strain of 0.1) data is shown in Fig. 8 as a function of temperature at 10^{-2} s^{-1} for all the materials. The flow stresses decreased monotonically with increasing temperature for the FSP 400/1 material and the parent material. On the other hand, flow stresses for the FSP 400/4 alloy decreased until 490 °C, but after that it increased again with temperature. However, with 200/4 FSP alloy, the flow stresses dropped gradually with increasing temperature up to 430 °C, but it increases at 450 °C. But, with further increase in temperature, the flow stresses came down again. It is important to note higher flow stresses for 200/4 material compared to other materials at higher temperatures (>430 °C).

However, the trend gets clear in Fig. 9, where ductility as a function of strain rate are plotted for the three FSP
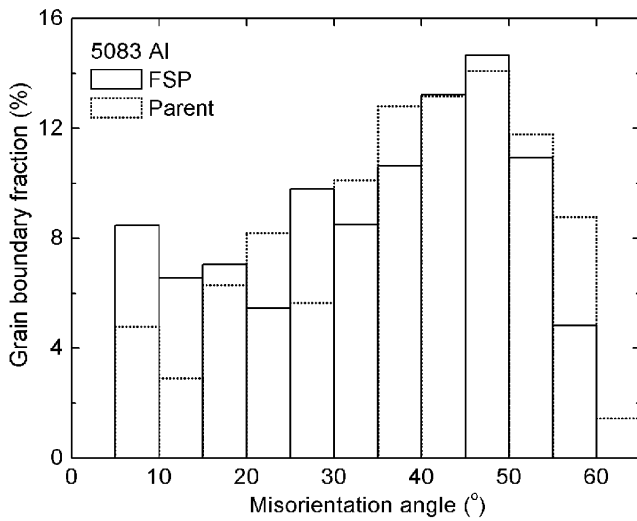
FIG. 5. Histograms of the grain boundary misorientation distribution in the parent and the FSP 400/1 5083 Al alloys as obtained from EBSD studies.

TABLE III. Summary of room temperature tensile properties of 5083 Al alloys.

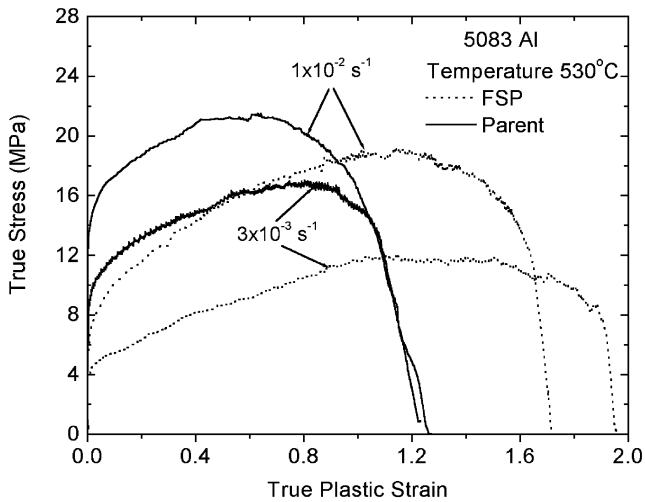| Alloy	Condition	Yield strength (MPa)	Ultimate tensile strength (MPa)	Elongation (%)
Parent 5083 Al	Partially recrystallized (rolled)	226	311	28.2
FSP 5083 Al	200 rpm, 101.6 mm/min	191	318	35.6
FSP 5083 Al	400 rpm, 25.4 mm/min	185	309	29.0
FSP 5083 Al	400 rpm, 101.6 mm/min	169	308	34.6

FIG. 6. Stress-strain curves for 5083 Al for the parent and FSP alloy (400/1).

alloys at their respective optimum superplastic temperatures. The FSP 400/1 alloy had the optimum ductility of 590% at a strain rate of 3×10^{-3} s^{-1} and 530 °C. In the same figure, the results of the parent material under
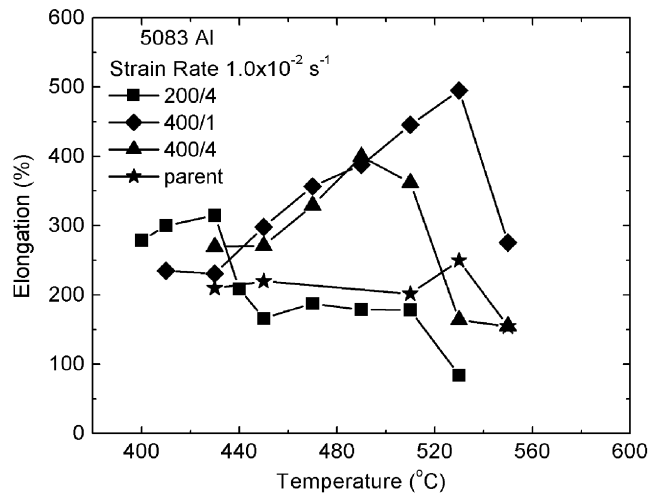

FIG. 7. The variation of ductility with temperature for the parent and the FSP 5083 alloys at a strain rate of 1×10^{-2} s^{-1}.
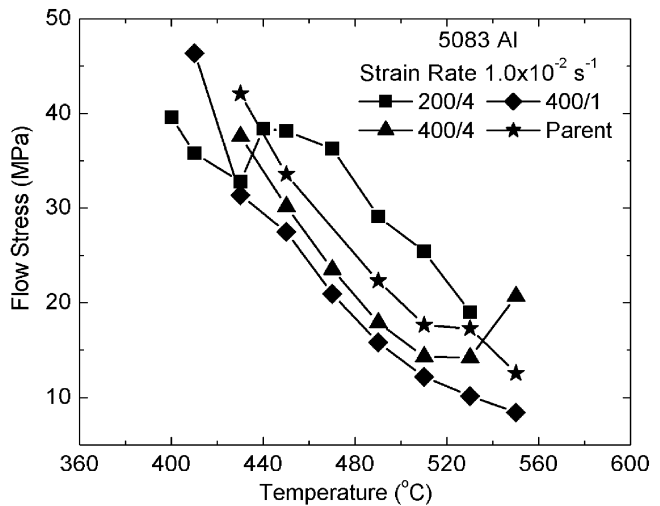

FIG. 8. Variation of flow stress with temperature for the parent and FSP 5083 alloys tested at an initial strain rate of 10^{-2} s^{-1}.

similar conditions are also plotted, and the FSP materials showed higher ductility than the parent material under similar conditions. The FSP 400/4 alloy had an optimum ductility of approximately 570% at a strain rate of 3×10^{-4} s^{-1}. Interestingly, the FSP 200/4 alloy with the smallest grain size (3.5 μm), exhibited only 315% maximum elongation at a strain rate of 10^{-2} s^{-1} and at 430 °C. However, at the highest strain rate investigated (10^{-1} s^{-1}), the ductility values (~150–250%) became moderate for all the materials.

Figure 10 shows the appearance of failed tensile specimens of 400/1 FSP alloy tested at 530 °C temperature and different strain rates. The uniformity in the deformed gage sections (except the specimen tested at 10^{-1} s^{-1}) is typical of superplastic deformation. However, all the ten sile specimens of the parent material deformed under similar conditions underwent significant necking (not shown).
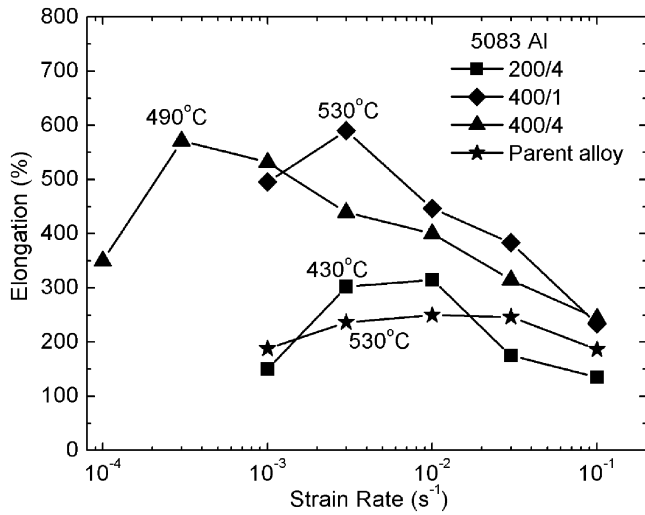
FIG. 9. Variation of ductility with strain rate for the FSP 5083 Al alloys at their respective optimum superplastic temperatures. Also, the data of the parent alloy at 530 °C is also shown.
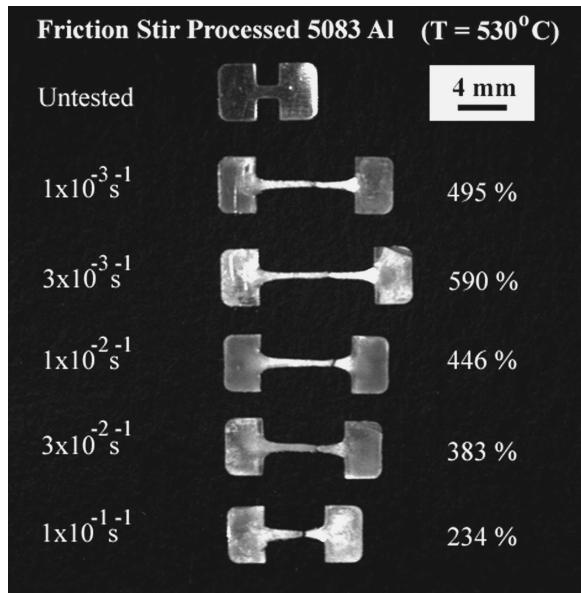

FIG. 10. Appearance of superplastically deformed tensile specimens of FSP 5083 Al (400/1). One undeformed specimen is also shown for comparison.

Figure 11(a) shows the variation of flow stress (at a true plastic strain of 0.1) against strain rate on a double logarithmic plot for both the parent and the 400/1 FSP materials at 530 °C. Additional data for the FSP 5083 Al obtained for the FSP alloy at 490 and 510 °C are shown. The apparent strain rate sensitivity value (m) for the FSP material was 0.52 in the superplastic strain rate range. On the other hand, for the parent material, the m value was about 0.32, which is clearly less than that of the FSP material. Figure 11(b) shows flow stresses as a function of strain rate for 200/4 and 400/4 FSP alloys at their respective optimum superplastic temperatures, that is,
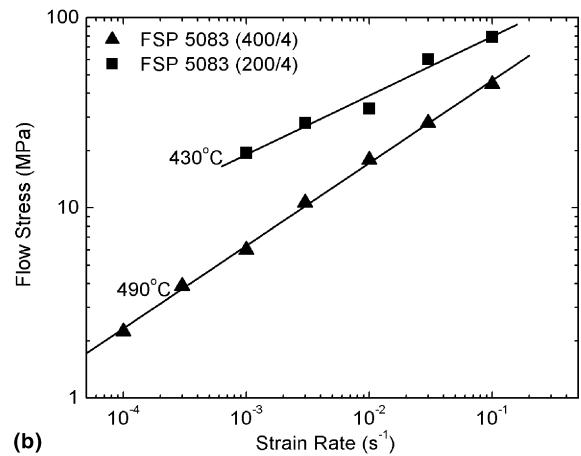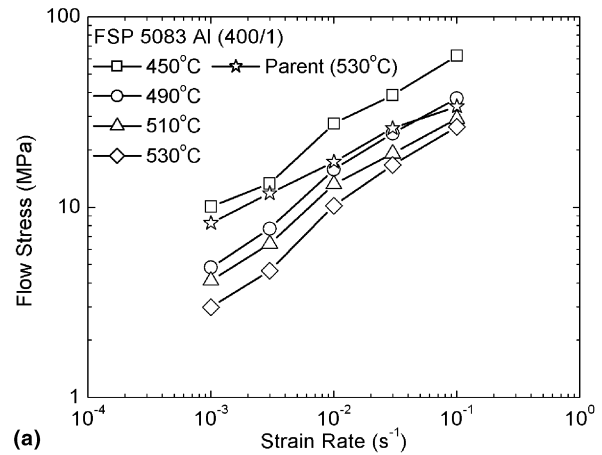
FIG. 11. Variation of flow stresses with initial strain rates (a) for the FSP 5083 Al (400/1) at different temperatures and the parent alloy at 530 °C, and (b) for 400/4 and 200/4 FSP 5083 Al alloys at their respective optimum superplastic temperatures.

430 and 490 °C. The m value for the 200/4 FSP alloy is much lower (0.31) than the 400/4 FSP alloy (0.44) at their respective optimum temperatures.

The value of apparent activation energy (Q) calculated for superplastic deformation in 400/1 FSP 5083 Al was about 98–106 kJ mol^{-1}, which is close to the activation energy for grain boundary self-diffusion (84 kJ mol^{-1}) in aluminum.[30] Similar calculations for the parent material yielded an activation energy of ~155 kJ mol^{-1} under similar conditions. This value is close to the activation energy of lattice self-diffusion for aluminum (142 kJ mol^{-1}).[30]

C. Cavitation behavior during superplastic deformation

Figure 12(a) shows an optical micrograph of a polished cross-section of a tensile specimen of 400/1 5083 Al pulled to failure under optimum conditions (530 °C, 3 × 10^{-3} s^{-1}). It shows that the cavity volume fraction (C$_v$) is very limited. On the other hand, the cross-section of a tensile specimen of the parent material pulled to failure

(a)

(b)

(c)

FIG. 12. Optical micrographs of polished cross-sections of tensile specimens of (a) the FSP 5083 Al deformed to failure at a temperature of 530 °C and a strain rate 3×10^{-3} s^{-1}, and (b) of the parent material deformed to failure under identical conditions. Note the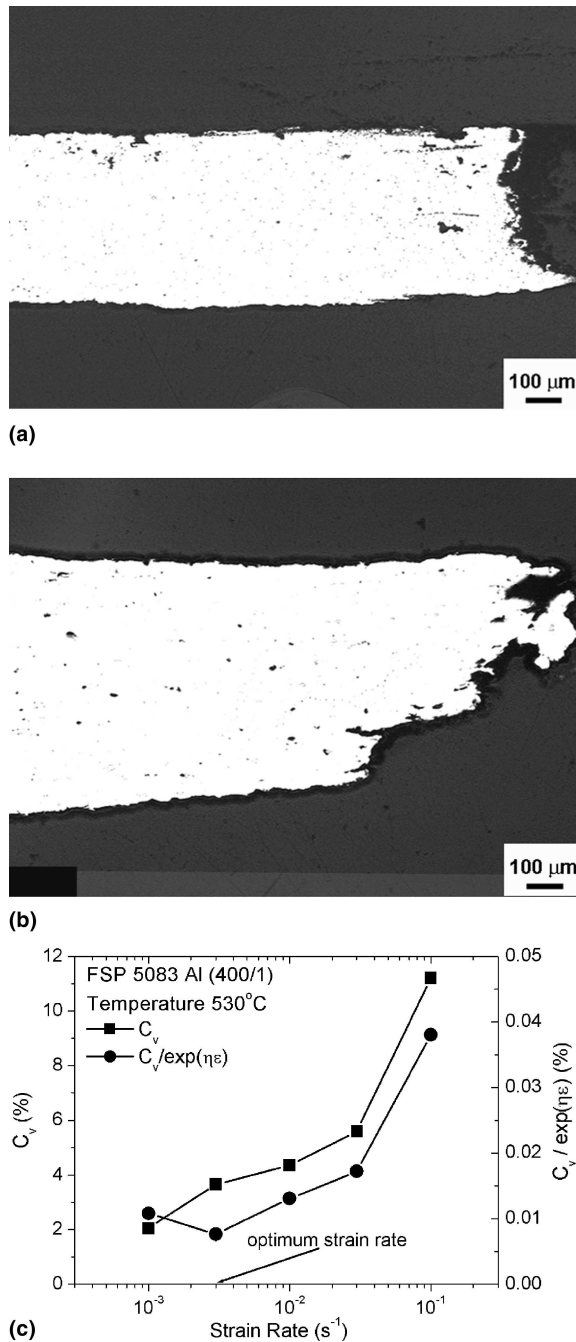 tensile axis is parallel to the horizontal. (c) Variation of cavity volume fraction and strain-normalized cavity volume fraction with strain rate for the FSP 5083 Al at 530 °C.

under similar conditions is shown in the optical micrograph of Fig. 12(b). The cavitation is also quite moderate in the FSP material as compared to the FSP alloy. However, unlike the parent material, there is a clear necking tendency in the deformed gauge of the parent material.

Figure 12(c) shows the cavity volume fraction near the fracture tip versus strain rate at 530 °C. It is observed that the cavity volume fraction increased monotonically with increasing strain rates. Strain-compensated cavity volume fraction is also plotted against the strain rate, and the rationale behind this analysis is given later.

IV. DISCUSSION

A. Microstructural evolution during FSP

Due to the high stacking fault energy of aluminum, it is difficult to refine the microstructure adequately through conventional TMP. Aluminum alloys exhibit accelerated recovery processes.[31,32] Consequently, there is no stored energy left to drive the recrystallization process for achieving significant grain refinement. That is why it takes several sequential TMP steps to obtain very fine recrystallized microstructures in aluminum alloys. In 5083 Al, the recrystallization is promoted at elevated temperatures (>250–300 °C) if it is properly cold-rolled. So, the mechanism responsible for grain refinement in the parent material is static recrystallization at shear bands or particle-stimulated recrystallization. Matsuo[33] reported that the multiple shear bands, that are formed during cold rolling in 5083 Al and due to the high Mg content of the matrix, could act as sites for recrystallization. Further, it was noted that the size and distribution of fine precipitates, amount of cold working and heating rate might determine the extent of grain refinement. Hence, grain sizes are often of the order 10–20 μm. The as-received material in the current study was in a partially recrystallized condition [Fig. 2(b)]. After conducting an annealing experiment, the parent material revealed fully recrystallized microstructure.

It is well known that the extent of grain refinement mostly determines the subsequent superplastic behavior. The processing techniques that can accumulate very high total plastic strains produce significant grain refinement.[34] In recent years based on this principle, severe plastic deformation (SePD) techniques have been developed to produce ultrafine grain microstructures (grain size <1 μm). Sato et al.[35] observed that FSW of annealed 5083 Al (with initial grain size of 18 μm) yielded a microstructure with approximately 4 μm grain size. Peel et al.[36] observed a grain size of 10–13 μm in friction stir welds of 5083-H19. Similarly, microstructures with fine grain sizes (3.5–8.5 μm) were obtained via FSP in the present investigation. The final grain size is likely to depend on the peak processing temperature and the cooling rate. The colder processing parameters (200/4) produced a finer grain size, whereas the hotter parameters (400/1) led to larger grain sizes (6.5 μm). From Fig. 1, it can be noted that the peak temperature for 200/4 was less (270 °C) compared to the peak temperature (530 °C) experienced in 400/1 material. Also, the time through

which the stirred material was at >200 °C is also more for hot processing parameters (400/1) than the cold parameters (200/4). Frigaard et al.[37] showed that if all the shearing work at the tool-shoulder interface gets converted into heat, the average heat input per unit area and time (Q) is given by

$$Q = (4/3)\pi^2\mu PNR^3 \quad , \tag{1}$$

where μ is the frictional coefficient, P the axial force, N the tool rotation rate, and R the tool shoulder radius. If it is assumed that the peak temperature scales directly with the heat input, doubling the tool rotation rate would lead to twice the increase in temperature. Likewise, the peak temperature measured for 400/1 FSP material was almost twice than that generated for 200/4 (Fig. 1). However, we want to emphasize here that FSP is a much more complex process, and making simple generalizations like this may not be valid. The final grain size may depend on the peak temperature, strain, strain rate and the cooling rate. But there is no physical relationship through which the grain size may be predicted. The complexity of the problem becomes evident with the 400/4 FSP material. The peak temperature is lower (475 °C) for the 400/4 material than the 400/1 material (530 °C), although following Eq. (1), identical temperature is predicted for both the runs. Also, the average grain size (8.5 μm) obtained in 400/4 FSP material is more than that of the 400/1 material (6.5 μm). A lower peak temperature and higher cooling rate in 400/4 material should have led to smaller grain size; however, that is not the case because of complex thermomechanical coupling. This particular aspect needs further investigation.

Unlike previous studies[24–26] where the FSP microstructure contained predominantly HAGBs, the FSP 5083 Al (400/1) contains at most 85% of HAGBs. Also, the GBMD is much like that of the recrystallized region of the parent material. Also, it can be pointed out that most of the previous studies only gave the GBMD of FSP materials, not the parent material. Interestingly, Karlsen et al.[38] have noted that a hot rolled 2024 Al (i.e., before FSW) also contained a rather large percentage of HAGBs (~95%). On the other hand, they estimated that 88–90% of the boundaries in the center of the processed region are high angled, quite similar to those found in other studies.[24–26] So, the generation of high grain boundary misorientation during FSP might need more careful examination. Nonetheless, it can be reasonably stated that the fine grain size with a large fraction of HAGBs decrease the effective grain size and thus would enhance superplasticity. Further, comparison with the study of Karlsen and co-workers[38] is not possible as they did not report the FSW parameters.

Larger intermetallic particles [such as Al_6(Mn,Fe)] get fragmented to smaller particles due to severe plastic deformation during FSP. There is no existing quantitative understanding of how the particle breakup is influenced by processing parameters or conditions. Often the size of particles appears to be important for breakup, and then material flow determines their final distribution. However, one trend has been noticed that higher tool rotation rates lead to better fragmentation. Particle size and distribution have implications for maximum achievable superplasticity since it influences the cavity nucleation process. This effect is discussed later.

Although the distinct microstructural evolution during FSP is not well understood, it is believed that dislocation glide-assisted subgrain rotation mechanism is responsible for the continuous dynamic recrystallization during FSP.[39] Few TEM studies[40,41] on the FSW microstructure revealed that despite the presence of dynamically recrystallized grains in the stirred region, there is a high density of residual dislocations. These dislocations are possibly generated by the forging action of the tool shoulder at the trailing edge.

Based on the mechanisms proposed by Jata and Semiatin[39] and Su et al.,[40] a plausible microstructural evolution mechanism during FSP of 5083 Al is discussed below:

(i) As the tool rotates and comes near the base material, the temperature in those regions rises significantly. As a result, the parent microstructure gets fully recrystallized before the tool possibly stirs the material.

(ii) Although the as-received parent material has regions of smaller subgrain features (0.5–0.8 μm), these subgrains are likely to transform to recrystallized grains. As this material comes in contact with the tool, shear deformation introduces new dislocations in the material, and new subgrains or cells start evolving inside those pre-existent statically recrystallized grains.

(iii) As it undergoes more deformation, additional dislocations get introduced into (sub)boundaries, converting them into high angle boundaries. Subgrain rotation takes place due to the chaotic mixing effect. Thus, dynamically recrystallized grains are formed.

(iv) As the tool leaves the material, an additional deformation effect through the forging action of the trailing edge of the tool shoulder leads to further dislocations being retained inside the grains (especially the larger grains).

(v) The thermal cycle persists for some time [as evident in Fig. 1(a)], possibly leading to the coarsening of grain size due to the concurrent non-isothermal grain growth, and should largely be controlled by the cooling rate.

B. Tensile properties

Li[42] suggested that a cold-rolled 5083 Al may start to statically recrystallize above a temperature of approximately 300 °C. Similar observations were made by Imamura and Ridley[2] and McQueen,[43] while heating a

cold-rolled 5083 Al to the tensile testing temperatures. In the current investigation, tensile tests were carried out in the temperature range of 410–550 °C. However, the appearance of highly elongated grains in the deformed sample (not shown) implies that the dominant deformation mechanism in the parent alloy is solute-drag dislocation glide (m = 0.32).[44]

As observed in Table III, room-temperature tensile properties of the FSP 5083 Al are not much different from its parent counterpart. Although the yield strength is little less than the parent material, the tensile strength and ductility values remained similar. It was observed that fine grain size (200/4, 3.5 μm) typically showed the highest yield strength, whereas the coarsest grain size gives the lowest following the well-known Hall-Petch relationship.

The current results demonstrate that enhanced superplastic properties could be obtained in the FSP 5083 Al. The general trend is that with decrease in grain size the optimum ductility is achieved at higher strain rates and/or lower temperatures. As evident in Figs. 7 and 9, the optimum ductility for the finest grain size (200/4, 3.5 μm) was obtained at a strain rate of 10^{-2} s^{-1} and at a low temperature of 430 °C. However, with increase in grain size, the optimum strain rate shifted to 3×10^{-3} s^{-1} (for 400/1, 6.5 μm) and to 3×10^{-4} s^{-1} (for 400/4, 8.5 μm). The ductility values for the FSP alloys were found to be higher than the parent material because of finer grain sizes.

However, it is important to note that 200/4 5083 Al with a finer grain size of 3.5 μm did not show better superplastic properties. It is also known that FSP microstructures in some FSP alloys become intrinsically unstable at elevated temperatures.[28,45–47] The origin of such thermal instability has been explained due to the loss of pinning forces and grain-size heterogeneity based upon Humphreys' microstructural stability model.[48] However, 5083 Al is a non–heat treatable alloy containing no metastable precipitates. This FSP alloy contained only fine, incoherent dispersoids of $Al_6(Mn,Cr)$ as the pinning agents. They do not go into solution or grow at 430 °C where the microstructural instability initiated. Hence, it is difficult to invoke any explanation involving pinning force loss due to the particle dissolution or coarsening in this alloy, as has been done for other heat-treatable Al alloys. However, Humphreys' model is applicable for microstructures where grain boundary migration is only dictated by grain boundary curvature. But it does not consider the effect of free dislocations. However, it has been noted in many reports that a slight deformation (less than what needed for recrystallization to occur) might initiate abnormal grain growth (AGG) in post-recrystallized microstructure.[49–51] As noted earlier, dynamically recrystallized FSP microstructure contains dislocations in a few larger grains due to the effect of tool

shoulder. For hot processing parameters (400/1 and 400/4), the dislocation density was much less presumably because of more time available at elevated temperatures for dislocation recovery during cooling. However, for colder parameters (200/4), faster cooling did not allow dislocations to undergo recovery, leaving a relatively larger dislocation density with a heterogeneous distribution. This might have led to AGG, with a few grains attaining some mobility advantage over other grains. This explanation would be attractive for explaining different AGG behavior with slight change in processing parameters. It can be noted that Peel et al.[36] have observed that the residual stress in the FSW of 5083 Al increases with increase in the traverse speed. Development of relationships between these features could offer an attractive explanation for AGG occurring in non-heat-treatable Al alloys, like in the current case.

The scanning electron microscopy (SEM) topographic image of a 200/4 FSP material tensile sample (pulled to failure at 450 °C and at a strain rate of 10^{-2} s^{-1}) near the fractured region is shown in Fig. 13. Relatively large elongated grains have consumed most of the finer grains of the as-FSP microstructure [Fig. 2(a)], and this resulted reduced ductility. Also, the elongated shapes of the abnormal grain indicate that dislocation glide mechanism was mainly operative in this region. This could be further understood from the variation of flow stress as a function of temperature as shown in Fig. 8. Similar observation was also made for a fine grained FSP 2024 Al (3.9-μm grain size) that showed abrupt increase in flow stress due to AGG.[26] The flow stress for 200/4 FSP alloy increased with increasing temperature above 430 °C, implying that most of finer grains might have been replaced by these larger grains. This is intriguing because the current material shows solute-drag dislocation creep behavior. This is supposed to be grain size independent. One possible explanation would be that the grain boundary area/unit
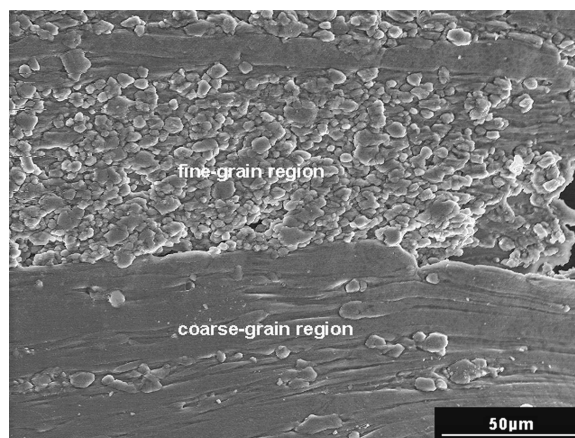

FIG. 13. A SEM topographical image of the FSP 5083 Al (200/4) tensile tested at a strain rate of 10^{-2} s^{-1} and 450 °C, showing the appearance of coarse grains in a matrix of fine grains.

volume might influence the source of dislocations. This might introduce a weak grain size dependence, but this aspect is not clear at this stage. With further increase in temperature, the flow stress gradually decreases indicating that all fine grains were lost. However, the flow stress values remained significantly above those of the other FSP materials, and even the parent material under similar testing conditions. On the other hand, for the 400/1 FSP and the parent materials, flow stress decreases monotonically with increasing temperature showing they are quite resistant to AGG. However, 400/4 material shows an increase in flow stress at a high temperature of >510 °C, with low ductility. Observation of the surface topography of the deformed sample revealed that this increase in flow stress was due to normal grain growth.

It is worth noting that approximately 400% ductility was also achieved at a high strain rate of 10^{-2} s^{-1} for 400/1 and 400/4 FSP 5083 Al alloys at 490 °C (Fig. 7). When compared to conventional superplastic 5083 Al alloys, FSP as a processing technique for superplasticity has certain advantages:

(i) Relatively thick plates of superplastic material (in the current study, 6.4 mm) can be produced (i.e., thick plate superplasticity can be achieved). In contrast, because most rolling-based TMP techniques need minimum true strain of approximately 2.3 to result into enough grain refinement, superplastic sheets of <3 mm are available, limiting its application only to sheet forming. Mahoney et al.[52] achieved thick plate (6.35 mm thick) superplasticity an FSP 7050 Al.

(ii) Chanda et al.[19] demonstrated that a two-step straining process is beneficial for attaining better superplastic response in a modified 5083 Al alloy. However, that might lead to complicated superplastic forming processes and interpretation of the results become difficult. Good superplastic properties were achieved in the current study with single strain rate straining.

(iii) Although SPD techniques take multiple cycles or passes to produce a microstructure suitable enough for superplasticity, FSP can take a single rastering pass to produce a microstructure that is amenable for superplasticity. However, scaling up to a larger quantity of alloy may need suitable overlapping schemes.

(iv) Another positive aspect of the high-temperature superplasticity observed is the low value of associated flow stress, which is very desirable for superplastic forming of components by using gas pressure. In the current study, the flow stresses for the FSP 5083 Al (such as 400/1 FSP alloy) under optimum superplastic conditions were <10 MPa.

It is well established that fine grain size (<15 μm) promotes structural superplasticity.[53] Matsuo et al.[33] noted that decreasing the grain size of a 5083 Al from approximately 24 μm to approximately 10 μm increases the elongation from about 150% to approximately 375%

at a temperature of 500 °C and strain rate of 3×10^{-3} s^{-1}. However, the finer grain size 3.5-μm FSP 5083 Al did not show an increase in ductility due to thermal instability, and this merits further investigation.

Watanabe[54] proposed grain boundary character distribution (GBCD) to introduce grain boundary engineering concept. In recent years, with the availability of more data on the GBCD of superplastic Al alloys, it is clear that HAGBs (particularly, the random or disordered ones), being able to slide significantly, influence superplastic properties. McNelley et al.[55] and Hirata et al.[56] found large population of high angled random boundaries present in the superplastic 5083 Al. The FSP alloy (400/1) has a large density of HAGBs (~85%) too, and thus, the superplastic properties were improved synergistically in the presence of fine grains.

C. Evaluation of flow properties and constitutive equations

Al–Mg alloys with coarse-grained microstructure are known to deform at high temperatures through a grain-size independent, solute-drag limited dislocation glide mechanism with a strain rate sensitivity value (m) of approximately 0.33.[44] Otsuka et al.[57] noted in an Al–5Mg alloy (both single and polycrystalline forms) the deformation mechanism did not change. This, in turn, supports the grain-size independent behavior of solute-drag dislocation glide mechanism. However, the ductility becomes less because of lower m-value than true superplasticity (m = 0.5). Taleff et al.[44,58] examined elevated temperature deformation of different coarse-grained Al–Mg alloys. Those alloys exhibited extended ductility with m-values of approximately 0.3. Similarly, in the current study, m-value for the parent alloy is 0.32. The FSP alloy with initial grain size of approximately 3.5 μm also has an apparent m value of 0.31. All these results with "extended ductility" values point toward the operation of a solute drag dislocation glide mechanism.

On the other hand, the m value for the FSP alloy under optimum conditions was found to be approximately 0.45–0.5 for 400/1 and 400/4 FSP alloys. An m value of 0.5 implies operation of a grain boundary sliding (GBS) deformation mechanism. It has been observed that different Al–Mg based alloys show optimum elongations of approximately 300% at an m value of ~0.3, whereas >400% requires m-values in the range of 0.4–0.7, which typically represent GBS dominated deformation behavior. This is a rough demarcation since total ductility is not a simple function of m only but depends also on the nature of failure mechanisms.

The most general constitutive relationship for high-temperature deformation could be expressed in the following form

$$\dot{\epsilon} = \frac{AD_o Eb}{kT} \left(\frac{\sigma}{E}\right)^n \left(\frac{b}{d}\right)^p \exp\left(\frac{-Q}{RT}\right) \quad , \qquad (2)$$

where $\dot{\epsilon}$ is the strain rate, σ the flow stress, A the dimensionless constant, Q the appropriate activation energy for the rate-limiting process, n the stress exponent (reciprocal to m), p the inverse grain size exponent, D_o the pre-exponential factor of diffusivity, T the temperature, E the Young's modulus, b the Burgers vector, k Boltzmann's constant, and R the universal gas constant. Most physically based superplasticity models predict an m value of 0.5 (i.e., n = 2) and p of 2.[53] Figure 14 shows modulus-compensated flow stress against normalized (i.e., grain size and temperature compensated) strain rate data for the FSP alloys (400/1 and 400/4). For this plot, p = 2 and n = 2 were used. The activation energy used was that of grain boundary self-diffusion for aluminum (84000 J/mol).[30] This analysis gives rise to the following constitutive equation for superplasticity in these FSP 5083 Al alloys

$$\dot{\epsilon} = \frac{232 D_{ogb} Eb}{kT} \left(\frac{\sigma}{E}\right)^2 \left(\frac{b}{d}\right)^2 \exp\left(\frac{-84000}{RT}\right) \quad . \qquad (3)$$

In Fig. 14, the constitutive equation proposed by Mishra et al.[59] for fine-grained aluminum alloys is included. The constitutive equation was of the same form as Eq. (2), but the constant value (A) was 40. The kinetics of superplasticity in FSP 5083 Al alloys appears to be faster than the observed value for conventional TMP aluminum alloys even on a normalized basis, whereas the data obtained by Kulas et al.[60] for a TMP 5083 Al ($\sim$7-μm grain size) more or less follow the conventional trend.

Recently, Ma et al.[27] obtained a larger constant value (A = 790) for superplastic FSP 7075 Al, as shown in Fig. 14. A dashed straight line representative of the equation derived by Ma et al.[27] is also shown in Fig. 14. It can be noted that the kinetics of superplastic flow in the FSP 7075 Al is faster than those obtained in the present study and in fine grained Al alloys.[59] It certainly points to some additional microstructural factors influencing the kinetics of these two FSP alloys, yet in the analysis those variations (such as grain boundary misorientations) could not be taken into account. The FSP 7075 Al investigated by Mishra et al.[24,25] contained approximately 95% of HAGBs, whereas the FSP 5083 Al (400/1) contained only $\sim$85% (Fig. 5). As noted earlier, grain boundary sliding occurs preferentially along HAGBs. It is likely that the larger fraction of HAGBs in the FSP alloy leads to faster kinetics. This field holds much promise in the concept that GBMD could be tailored to produce even better superplastic aluminum alloys through FSP.

FSP 200/4 and parent 5083 alloys exhibit apparent m values of approximately 0.3. To check how the results scale with the data of other Al-Mg alloys from different studies,[58,61–63] and the theoretical prediction for the solute drag creep equation,[64,65] all the data of FSP 200/4 and the parent materials are plotted on a normalized basis in Fig. 15. Mg has a particularly high misfit parameter. This effect leads to diffusion of Mg solute to dislocation cores forming a saturated atmosphere of solute and imposes drag force. The form of the equation used was the same except that p was taken as zero (i.e., no grain size dependence). The activation energy used here is that for the lattice self-diffusion of Al (142000 J/mol).[30] Strictly, the diffusivity should be the diffusivity of Mg in Al lattice.
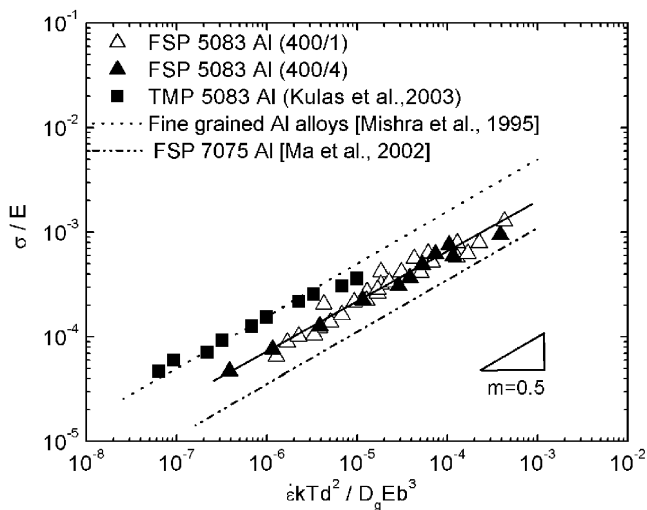

FIG. 14. A normalized flow stress versus normalized strain rate plot, giving rise to the appropriate constitutive equation for the FSP 5083 Al alloys (400/1 and 400/4). Note that the constitutive equations proposed by Mishra et al.[59] for fine-grained Al alloys, and by Ma et al.[27] for FSP 7075 Al alloys, and data from Kulas et al.[60] are also shown for comparison.
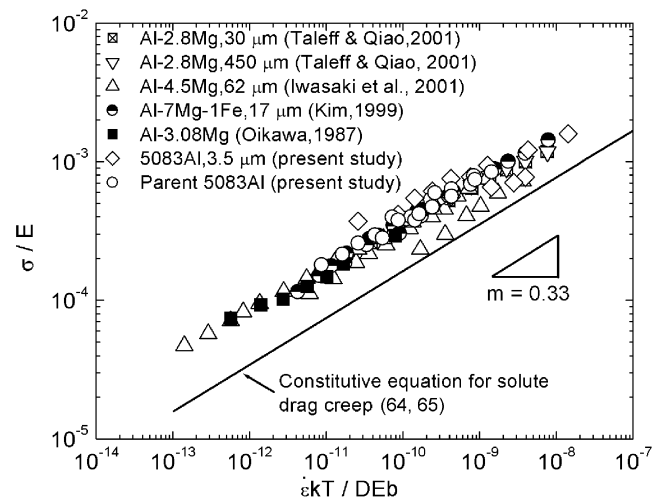

FIG. 15. Normalized flow stress versus normalized strain rate data from different studies related to Al–Mg alloys including the current data from the FSP 200/4 and the parent materials. Note that the two straight lines shown follows the constitutive equation proposed for solute drag creep (A = 25).

It could be noted here that an activation energy of ~150 kJ/mol was obtained for the parent 5083 Al. Hence, Q was taken as 142 kJ/mol so that all these diverse data could be compared from different studies. The analysis in Fig. 15 shows that all data fall in close proximity with the data of the parent and FSP 200/4 5083 Al alloys, which also fall close to the data using equation constant (A = 25) calculated by Bieler and Mukherjee[64] based on the theoretical prediction of the viscous glide creep given by Weertman and Weertman.[65] Thus, a constitutive relation for the 5083 Al (parent and 200/4 FSP) following a solute-drag type dislocation glide mechanism is

$$\dot{\epsilon} = \frac{2D_{oL}Eb}{kT} \left(\frac{\sigma}{E}\right)^3 \exp\left(\frac{-142000}{RT}\right) \quad , \qquad (4)$$

where D_{oL} is the appropriate frequency factor for lattice diffusion in aluminum and all other terms have their usual meaning.

D. Significance of cavitation

In this study, cavitation experiments were conducted only for the FSP 400/1 5083 Al and the parent alloy. Often cavities are nucleated at grain boundary ledges and triple points and coarser second phase particles situated at grain boundaries.[66] Most studies agree that coarse second phase particles are the preferred sites where cavities nucleate. Cavities initiate at the interface of the matrix and the particle under the action of tensile stresses, resulting into debonding or decohesion. If the particle size is larger, the accommodation process through diffusion and/or dislocation motion for suppressing cavity nucleation becomes insufficient. Matsuo[33] observed that the tendency toward cavitation increased with increasing iron and silicon contents in 5083 Al and adversely influenced formability. Taleff et al.[67] performed a detailed study on the cavitation behavior of coarse-grained Al-Mg alloys. They found that both necking-controlled and cavitation-controlled failure processes could occur depending on the testing conditions, and alloy chemistry (i.e., second phase particles).

In the current study, the size and distribution of primary intermetallic phases, Al_6(Mn,Fe) and Al–Mn–Fe–Si, are different before and after FSP [Figs. 4(a) and 4(b), respectively]. A previous study on 2024 Al established that FSP could bring about substantial changes in size and spatial distribution of constituent particles.[47] In a recent study, it was shown that the cavitation level in the FSP 7075 Al alloy is substantially less than conventionally processed superplastic 7475 Al alloy.[68] Here, it is found that the cavitation level of FSP 5083 Al (400/1) is less than the parent material [Figs. 12(a) and 12(b)] under similar deformation conditions, probably because necking is more dominant as a failure process in the parent material.

Cavities have irregular, jagged boundaries in the FSP alloy, possibly, as a consequence of plasticity-controlled cavity growth.[66] Figure 12(c) shows the variation of cavity volume fraction at the proximity of the fracture surfaces increased with increasing strain rate due to the associated increase in flow stress [Fig. 11(a)]. However, it has been noted in several studies that the cavity volume fraction also depends on the local strain experienced at deformed gage length. Hancock[69] derived an expression relating cavity volume fraction (C_v) and the true strain (ϵ) as

$$C_v = C_o \exp(\eta\epsilon) \quad , \qquad (5)$$

where η is the cavity growth rate parameter and C_o is a pre-exponential constant. Hence, a normalized cavity volume fraction given by $C_v/\exp(\eta\epsilon)$ could be used to take into account the effect of strain. Note that the value of η is considered constant as calculated from the following equation given by Cocks and Ashby[70] and Stowell[71]

$$\eta = \frac{3}{2}\left(\frac{m+1}{m}\right)\left[\sinh\left(\frac{2(2-m)}{2+m}\right)\frac{k_s}{3}\right] \quad . \qquad (6)$$

where k_s is a geometry factor whose value depends on the test condition and the extent of grain boundary sliding. Although experimental η has been found to change with increase in strain rate in previous studies within 1–3, it was calculated to be 2.87 from Eq. (6). The k_s value was taken as 1.5 (good for uniaxial tension) and m value of 0.5, which was experimentally determined for FSP 400/1 5083 Al. It can be noted from Fig. 13(c), the function [$C_v/\exp(\eta\varepsilon)$] has the lowest value at the optimum strain rate (3×10^{-3} s^{-1}). Hence, although cavity volume fraction increased with strain rate, when normalized by strain, the cavitation is minimum at the strain rate where maximum ductility (590%) was obtained.

V. CONCLUSIONS

(1) The microstructure of the FSP alloys consisted of fine dynamically recrystallized grains (~3.5–8.5 μm).

(2) The 400/1 FSP 5083 Al showed optimum superplasticity (590%) at a strain rate of 3×10^{-3} s^{-1} and temperature of 530 °C, whereas the 400/4 FSP 5083 Al showed ~570% at a strain rate 3×10^{-4} s^{-1} and 490 °C. The FSP alloy with the finest grains (FSP 200/4, 3.5-μm grain size) exhibited less optimum ductility of 315% at a higher strain rate of 10^{-2} s^{-1} and at a lower temperature of 430 °C, due to enhanced microstructural instability.

(3) GBS-related deformation mechanism was found to be associated with the superplastic deformation of FSP 5083 Al alloys (400/1 and 400/4), whereas solute drag dislocation glide mechanism was the dominant deformation mechanism for the 200/4 and parent alloys.

(4) FSP parameters need careful optimization, as they have major effects on the thermal stability and superplastic properties even when room temperature properties are not affected much.

ACKNOWLEDGMENTS

REFERENCES

1. A.J. Barnes: Superplastic aluminum forming – expanding its techno-economic niche. *Mater. Sci. Forum* **304–306,** 785 (1999).
2. H. Imamura and N. Ridley: In *Superplasticity in Advanced Materials*, edited by S. Hori, M. Tokizane, and N. Furoshiro (JSRS Symp. Proc., Tokyo, Japan, 1991), p. 453.
3. R. Verma, A.K. Ghosh, S. Kim, and C. Kim: Grain refinement and superplasticity in 5083 Al. *Mater. Sci. Eng. A* **191,** 143 (1995).
4. J. Pimenoff, Y. Yagodzinskyy, J. Romu, and H. Hanninen: Effects of the temperature of warm rolling on the superplastic behavior of AA5083 aluminium base alloy. *Mater. Sci. Forum* **357–359,** 277 (2001).
5. M.T. Perez-Prado, G. Gonzalez-Doncel, O.A. Ruano, and T.R. McNelley: Texture analysis of the transition from slip to grain boundary sliding in a discontinuously recrystallized superplastic aluminum alloy. *Acta Mater.* **49,** 2259 (2001).
6. I.C. Hsiao and J.C. Huang: Deformation mechanisms during low- and high-temperature superplasticity in 5083 Al-Mg alloy. *Metall. Mater. Trans.* **33A,** 1373 (2002).
7. H. Iwasaki, H. Hosokawa, T. Mori, T. Tagata, and K. Higashi: Quantitative assessment of superplastic deformation behavior in a commercial 5083 alloy. *Mater. Sci. Eng. A* **252,** 199 (1999).
8. L. Dupuy, J.J. Blandin, and E.F. Rauch: Structural and mechanical properties in AA 5083 processed by ECAE. *Mater. Sci. Technol.* **16,** 1256 (2000).
9. J.W. Sinclair, K.T. Hartwig, Jr., R.E. Goforth, E.A. Kenik, and E. Voelkl: In *Ultrafine Grained Materials*, edited by R.S. Mishra, S.L. Semiatin, C. Suryanarayana, N.N. Thadhani, and T.C. Lowe (TMS, Warrendale, PA, 2000), p. 393.
10. D.R. Herling and M.T. Smith: In *Ultrafine Grained Materials*, edited by R.S. Mishra, S.L. Semiatin, C. Suryanarayana, N.N. Thadhani, and T.C. Lowe (TMS, Warrendale, PA, 2000), p. 411.
11. K.T. Park, D.Y. Hwang, S.Y. Chang, and D.H. Shin: Low-temperature superplastic behavior of a submicrometer-grained 5083 Al alloy fabricated by severe plastic deformation. *Metall. Mater. Trans.* **33A,** 2859 (2002).
12. N. Tsuji, K. Shiotsuki, and Y. Saito: Superplasticity of ultra-fline grained Al-Mg alloy produced by accumulative roll-bonding. *Mater. Trans. (JIM)* **40,** 765 (1999).
13. H. Watanabe, K. Ohori, and Y. Takeuchi: Superplastic behavior of Al–Mg–Cu alloys. *Trans. Iron Steel Inst., Japan.* **27,** 730 (1987).
14. F. Li, D.H. Bae, and A.K. Ghosh: Grain elongation and anisotropic grain growth during superplastic deformation in an Al-Mg-Mn-Cu alloy. *Acta Mater.* **45,** 3887 (1997).
15. K. Kannan, C.H. Johnson, and C.H. Hamilton: A study of superplasticity in a modified 5083 Al-Mg-Mn alloy. *Metall. Mater. Trans.* **29A,** 1211 (1998).
16. J.S. Vetrano, C.H. Henager, Jr., and S.M. Bruemmer: In *Superplasticity and Superplastic Forming*, edited by A.K. Ghosh and T.R. Bieler (TMS, Warrendale, PA, 1998), p. 89.
17. C.H. Henager, Jr., J.S. Vetrano, V.Y. Gertsman, and S.M. Bruemmer: In *Superplasticity—Curent Status and Future Potential,* edited by P.B. Berbon, M.Z. Berbon, T. Sakuma, and T.G. Langdon (Mater. Res. Soc. Symp. Proc. **601,** Warrendale, PA, 2000), p. 31.
18. R.O. Kaibyshev and F.F. Musin: Subsolidus superplasticity. *Doklady Physics* **45,** 324 (2000).
19. T. Chanda, A.K. Ghosh, and C. Lavender: In *Superplasticity and Superplastic Forming*, edited by A.K. Ghosh and T.R. Bieler (TMS, Warrendale, PA, 1995), p. 49.
20. K. Higashi, S. Tanimura, and T. Ito: In *Superplasticity in Metals, Ceramics, and Intermetallics*, edited by M.J. Mayo, M. Kobayashi, and J. Wadsworth (Mater. Res. Soc. Proc. **196,** Pittsburgh, PA, 1990), p. 385.
21. R. Grimes, R.J. Dashwood, A.W. Harrison, and H.M. Flower: Development of a high strain rate superplastic Al-Mg-Zr alloy. *Mater. Sci. Technol.* **16,** 1334 (2000).
22. K.T. Park, D.H. Hwang, Y.K. Lee, Y.K. Kim, and D.H. Shin: High strain rate superplasticity of submicrometer grained 5083 Al alloy containing scandium fabricated by severe plastic deformation. *Mater. Sci. Eng. A* **341,** 273 (2003).
23. W.M. Thomas, E.D. Nicholas, J.C. Needham, M.G. Murch, P. Templesmith, and C.J. Dawes: "Friction Stir Butt Welding." G.B. Application No. 9125978.8, Dec. 1991; U.S. Patent No. 5460317, Oct. 1995.
24. R.S. Mishra, M.W. Mahoney, S.X. McFadden, N.A. Mara, and A.K. Mukherjee: High strain rate superplasticity in a friction stir processed 7075 Al alloy. *Scripta Mater.* **42,** 163 (2000).
25. R.S. Mishra and M.W. Mahoney: Friction stir processing: A new grain refinement technique to achieve high strain rate superplasticity in commercial alloys. *Mater. Sci. Forum* **357–359,** 507 (2001).
26. I. Charit and R.S. Mishra: High strain rate superplasticity in a commercial 2024 Al alloy via friction stir processing. *Mater. Sci. Eng. A* **359,** 290 (2003).
27. Z.Y. Ma, R.S. Mishra, and M.W. Mahoney: Superplastic deformation behavior of friction stir processed 7075Al alloy. *Acta Mater.* **50,** 4419 (2002).
28. Z.Y. Ma, R.S. Mishra, M.W. Mahoney, and R. Grimes: High strain rate superplasticity in friction stir processed Al-Mg-Zr alloy. *Mater. Sci. Eng. A* **351,** 148 (2003).
29. I. Charit and R.S. Mishra: In *Ultrafine Grained Materials III*, edited by Y.T. Zhu, T.G. Langdon, R.Z. Valiev, S.L. Semiatin, D.H. Shin, and T.C. Lowe (TMS, Warrendale, PA, 2004), p. 95.
30. H.J. Frost and M.F. Ashby: *Deformation Mechanism Maps* (Pergamon Press, London, U.K., 1985), p. 21.
31. F.J. Humphreys and M. Hatherly: *Recrystallization and Related Annealing Phenomenon* (Pergamon Press, London, U.K., 2002), p. 128.
32. J.C. Williams and E.A. Starke, Jr.: In *Deformation, Processing and Structure*, edited by G. Krauss (ASM, Metals Park, OH, 1982) p. 279.
33. M. Matsuo: In *Superplasticity: 60 years after Pearson*, edited by N. Ridley (Maney Publisher, London, U.K., 1995), p. 277.
34. F.J. Humphreys, P.B. Prangnell, J.R. Bowen, A. Gholinia, and C. Harris: Developing stable fine grain microstructures by large strain deformation. *Phil. Trans. A (Royal Society)* **357,** 1663 (1999).

35. Y.S. Sato, S.H.C. Park, and H. Kokawa: Microstructural factors governing hardness in friction-stir welds of solid-solution-hardened Al alloys. *Metall. Mater. Trans.* **32A,** 3033 (2001).

36. M. Peel, A. Steuwer, M. Preuss, P.J. Withers: Microstructure, mechanical properties and residual stresses as a function of welding speed in aluminium AA5083 friction stir welds. *Acta Mater.* **51,** 4791 (2003).

37. O. Frigaard, O. Grong, and O.T. Midling: A process model for friction stir welding of age hardening aluminium alloys. *Metall. Mater. Trans.*, **32A,** 1189 (2001).

38. M. Karlsen, O. Frigaard, H. Hjelen, O. Grong, and H. Norum: SEM-EBSD - characterisation of the deformation microstructure in friction stir welded 2024 T351 aluminium alloy. *Mater. Sci. Forum* **426–432,** 2861 (2003).

39. K.V. Jata and S.L. Semiatin: Continuous dynamic recrystallisation during friction stir welding of high strength aluminium alloys. *Scripta Mater.* **43,** 743 (2000).

40. J.Q. Su, T. W. Nelson, R. Mishra, and M. Mahoney: Microstructural investigation of friction stir welded 7050-T651 aluminium. *Acta Mater.* **51,** 713 (2003).

41. B. Heinz and B. Skrotzki: Characterisation of a friction-stir-welded aluminium alloy 6013. *Metall. Mater. Trans.* **33B,** 489 (2002).

42. F. Li: Microstructural evolution and mechanisms of superplasticity in an Al-4.5% Mg alloy. *Mater. Sci. Technol.* **13,** 17 (1997).

43. H.J. McQueen: In *Materials in Automotive Industry*, edited by E. Essadiai, F.E. Goodwin, and M. Elboujdaini, (Canadian Metal Society, Toronto, Canada, 2001), p. 279.

44. E.M. Taleff: In *Creep Behavior of Advanced Materials for the 21st Century*, edited by R.S. Mishra, A.K. Mukherjee, and K.L. Murty (TMS, Warrendale, PA, 1999), p. 349.

45. I. Charit, R.S. Mishra, and M.W. Mahoney: Multi-sheet structures in 7475 aluminum by friction stir welding in concert with post-weld superplastic forming. *Scripta Mater.* **47,** 631 (2002).

46. R.S. Mishra, R.K. Islamgaliev, T.W. Nelson, Y. Hovansky, and M.W. Mahoney: In *Friction Stir Welding and Processing*, edited by K.V. Jata, M.W. Mahoney, R.S. Mishra, S.L. Semiatin, and D.P. Field (TMS, Warrendale, PA, 2001), p. 205.

47. I. Charit, Z.Y. Ma, and R.S. Mishra: In *Hot Deformation of Aluminum Alloys III*, edited by Z. Jin, A. Beaudoin, T.A. Bieler, and B. Radhakrishnan (TMS, Warrendale, PA, 2003), p. 331.

48. F.J. Humphreys: A unified theory of recovery, recrystallisation and grain growth, based on the stability and growth of cellular microstructures. *Acta Mater.* **45,** 5031 (1997).

49. V. Randle and A. Brown: The effects of strain on grain misorientation texture during the grain growth incubation Period. *Philos. Mag. A* **58,** 717 (1988).

50. C. Antonione, F. Marino, G. Riontino, and M.C. Tabasso: Effect of slight deformations on grain growth in iron. *J. Mater. Sci.* **12,** 747 (1977).

51. J.B. Koo, D.H. Yoon, and M.F. Henry: The effect of small deformation on abnormal grain growth in bulk Cu. *Metall. Mater. Trans.* **33A,** 3803 (2002).

52. M. Mahoney, R.S. Mishra, T. Nelson, J. Flintoff, R. Islamgaliev, and Y. Hovansky: In *Friction Stir Welding and Processing*, edited by K.V. Jata, M.W. Mahoney, R.S. Mishra, S.L. Semiatin, and D.P. Field (TMS, Warrendale, PA, 2001), p. 183.

53. O.D. Sherby and J. Wadsworth: Superplasticity- recent advances and future directions. *Prog. Mater. Sci.* **33,** 169 (1989).

54. T. Watanabe: Key issues of grain boundary engineering for superplasticity. *Mater. Sci. Forum* **243–245,** 21 (1997).

55. T.R. McNelley, M.E. McMohan, and S.J. Hales. An EBSP investigation of alternate microstructures for superplasticity in aluminum-magnesium alloys. *Scripta Mater.* **36,** 369 (1997).

56. T. Hirata, T. Osa, H. Hosokawa, and K. Higashi: Effects of flow stress and grain size on the evolution of grain boundary microstructure in superplastic 5083 aluminum alloy. *Mater. Trans. (JIM)* **43,** 2385 (2002).

57. M. Otsuka, S. Shibasaki, and M. Kikuchi: Superplasticity in coarse grained Al-Mg alloys. *Mater. Sci. Forum* **233–234,** 193 (1997).

58. E.M. Taleff and J. Qiao: In *Light Metals 2001*, edited by M. Sahoo and T.J. Lewis. (Canadian Institute of Mining, Metallurgy and Petroleum, Montreal, Canada, 2001), p. 77.

59. R.S. Mishra, T.R. Bieler, and A.K. Mukherjee: Superplasticity in powder-metallurgy alumunum-alloys and composites. *Acta Metall. Mater.* **43,** 877 (1995).

60. M.A. Kulas, P.E. Krajewski, T. McNelley, and E.M. Taleff: In *Hot Deformation of Aluminum Alloys III*, edited by Z. Jin, A. Beaudoin, T.R. Bieler, and B. Radhakrishnan (TMS, Warrendale, PA, 2003), p. 499.

61. H. Iwasaki, R. Kariya, M. Mabuchi, T. Tagata, and K. Higashi: Effects of flow stress and grain size on the evolution of grain boundary microstructure in superplastic 5083 aluminum alloy. *Mater. Trans. (JIM)* **42,** 1771 (2001).

62. W.J. Kim: Role of subgrain formation in high strain rate superplasticity of Al-Mg alloy. *Mater. Sci. Forum* **304–306,** 273 (1999).

63. H. Oikawa: In *Creep and Fracture of Engineering Materials and Structures*, edited by B. Wilshire and R.W. Evans (The Institute of Metals, London, 1987), p. 99.

64. T.R. Bieler and A.K. Mukherjee: The high strain rate superplastic deformation mechanisms of mechanically alloyed aluminum IN90211. *Mater. Sci. Eng. A* **128,** 171 (1990).

65. J. Weertman and J.R. Weertman: In *Constitutive Relations and Their Physical Basis*, edited by S.I. Andersen, J.B. Slide-Sorensen, N. Hansen, T. Leffers, H. Lilholt, O.B. Pederson, and B. Ralph (RISO National Laboratory, Roskilde, Denmark, 1987), p. 191.

66. N. Ridley and Z.C. Wang: Cavitation in superplastic materials. *Mater. Sci. Forum* **170–172,** 177 (1994).

67. E.M. Taleff, D.R. Leuser, C.K. Syn, and G.A. Henshall: In *Recent Advances in Fracture*, edited by R.K. Mahidhara, A.B. Geltmacher, P. Matic, and K. Sadananda (TMS, Warrendale, PA, 1997), p. 295.

68. Z.Y. Ma and R.S. Mishra: Cavitation in superplastic 7075Al alloys prepared via friction stir processing. *Acta Mater.* **51,** 3551 (2003).

69. J.W. Hancock: Creep cavitation without a vacancy flux. *Met. Sci.* **10,** 319 (1976).

70. A.C.F. Cocks and M.F. Ashby: Creep fracture by coupled power-law creep and diffusion under multiaxial stress. *Met. Sci.* **16,** 465 (1982).

71. M.J. Stowell: Cavity growth in superplastic alloys. *Met. Sci.* **14,** 267 (1980).